



**HAL**  
open science

# Effects of Andrade and Burgers rheologies on glacial isostatic adjustment modeling in Antarctica

Alexandre Boughanemi, Anthony Mémin

► **To cite this version:**

Alexandre Boughanemi, Anthony Mémin. Effects of Andrade and Burgers rheologies on glacial isostatic adjustment modeling in Antarctica. *Geodesy and Geodynamics*, inPress, 10.1016/j.geog.2023.12.008 . hal-04531748

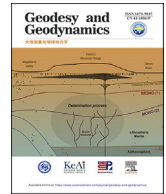
**HAL Id: hal-04531748**

**<https://hal.science/hal-04531748>**

Submitted on 4 Apr 2024

**HAL** is a multi-disciplinary open access archive for the deposit and dissemination of scientific research documents, whether they are published or not. The documents may come from teaching and research institutions in France or abroad, or from public or private research centers.

L'archive ouverte pluridisciplinaire **HAL**, est destinée au dépôt et à la diffusion de documents scientifiques de niveau recherche, publiés ou non, émanant des établissements d'enseignement et de recherche français ou étrangers, des laboratoires publics ou privés.



# Effects of Andrade and Burgers rheologies on glacial isostatic adjustment modeling in Antarctica

Alexandre Boughanemi\*, Anthony Mémin

Université Côte d'Azur, CNRS, Observatoire de la Côte d'Azur, IRD, Géoazur, 250 rue Albert Einstein, Sophia Antipolis 06560 Valbonne, France

## ARTICLE INFO

### Article history:

Received 4 May 2023

Accepted 27 December 2023

Available online xxx

### Keywords:

GIA  
 Antarctica  
 Modeling  
 Rheology  
 Displacement  
 Viscosity  
 GNSS

## ABSTRACT

Variations in ice mass deform the Earth and modify its gravity field, a process known as Glacial Isostatic Adjustment (GIA). GIA in Antarctica remains poorly constrained due to the cumulative effect of past and present ice-mass changes, the unknown history of the past ice-mass change, and the uncertainties on the mechanical properties of the Earth. This paper investigates the effect of using Andrade and Burgers viscoelastic rheologies, rather than the commonly used Maxwell rheology, to model GIA-induced deformation in Antarctica. The Love number and Green's function formalism are used to compute the radial surface displacements and the gravity changes induced by the past and present ice-mass changes. We consider an Earth model whose elastic properties and radial structure are averaged from the Preliminary Reference Earth Model and two viscosity profiles to account for the recently published results on the present ice-mass changes. Using the three rheological laws affects the temporal response of the Earth differently, leading to smaller discrepancies than those induced by the two viscosity structures. The differences are the largest between Maxwell and Burgers rheologies during the 100–1000 years following the beginning of the surface-mass change. Results show that using the Andrade and Burgers rheologies allows the Earth to respond on decennial to centennial time scales, up to 10 m more than Maxwell. Considering only the recent ice-mass changes, the deformation rates derived from Burgers and Andrade rheologies are several times larger than those estimated by Maxwell rheology.

© 2024 Editorial office of Geodesy and Geodynamics. Publishing services by Elsevier B.V. on behalf of KeAi Communications Co. Ltd. This is an open access article under the CC BY-NC-ND license (<http://creativecommons.org/licenses/by-nc-nd/4.0/>).

## 1. Introduction

Antarctica is the southernmost continent on Earth. Its surface covers  $14.1 \times 10^6$  km<sup>2</sup> including 98% beneath ice. The melting of the Antarctic Ice Sheet (AIS) could induce a global mean sea level rise of 58 m [1]. Due to the large extent of the AIS, ice-mass change can only be assessed from satellite altimetry data, which provides changes in the elevation of the ice surface, or by satellite gravimetry data, where changes in gravity are a direct result of changes in mass [2,3]. Several studies provide estimates of the ice mass balance in Antarctica [1,4]. The results indicate an ice loss of about 2,720 Gt

between 1992 and 2017 [1]. In response to these mass changes, the surface of the Earth deforms. Deformations resulting from past and present ice-mass changes are due to viscoelastic processes and gravitational responses, tending to an isostatic equilibrium. This process, called Glacial Isostatic Adjustment (GIA), is directly influenced by the mechanical properties and the structure of the inner Earth.

The effects of GIA have been observed and studied for a long time [5,6]. GIA generates crustal displacements and variations of the Earth's gravity field, which are currently observed by the Global Navigation Satellite System (GNSS) and ground or space-based gravimetry such as the Gravity Recovery and Climate Experiment (GRACE) and its Follow On (GRACE-FO) missions [7,8]. Removing GIA signals from positioning and gravity data is required to accurately estimate present ice-mass changes from geodetic observations [9–11]. GIA-induced deformations are classically modeled by assuming a viscoelastic Earth with a Maxwell rheology [9,12,13]. This rheology is characterized by a short-term elastic response and a long-term viscous response, commonly represented as a spring and a dash-pot, respectively. The Maxwell rheology has made it possible to explain the sea level evolution deduced from the

\* Corresponding author.

E-mail address: [alexandre.boughanemi@geoazur.unice.fr](mailto:alexandre.boughanemi@geoazur.unice.fr) (A. Boughanemi).

Peer review under responsibility of Institute of Seismology, China Earthquake Administration.



emergence of paleo-shorelines, particularly in regions formerly covered by ice during the Last Glacial Maximum (LGM), such as the North American region [14]. Several studies based on GIA-related observations, such as land uplift or relative sea level, suggest that the average viscosity of the mantle, from the bottom of the lithosphere down to a depth of 1 400 km, should be of the order of  $10^{21}$  Pa·s [15,16]. However, recent studies show that uplift rates in response to current glacier thinning [17] and those resulting from the end of the Little Ice Age (LIA) [18–20] cannot be explained by the Maxwell rheology and the classical viscosity profile used to describe the deformations resulting from the Pleistocene deglaciation. These deformations are best explained if a viscosity of about  $10^{18} - 10^{19}$  Pa·s is used for the upper mantle or a part of it. In Antarctica, such low viscosities might reflect the lateral structure of the Earth as suggested by seismic tomography [21,22]. It has already been shown that lateral changes in the Earth's mechanical structure can affect the predictions of surface displacement [10], mass balance from space-based gravimetry [23], and sea-level change [24]. However, they remain barely considered when analyzing geodetic data or deriving the global deglaciation model ICE6G\_C [25].

In parallel, studies of postseismic deformation commonly employ Burgers rheology [26], suggesting lower viscosities and fast non-elastic deformations. The Burgers rheology can be described as a Maxwell element (spring and dash-pot in series) and one (simple Burgers model or SBM) or several (extended Burgers model or EBM) Kelvin-Voigt elements (spring- and dash-pot in parallel) connected in series. Maxwell and Kelvin-Voigt elements allow SBM and EBM to describe steady-state and transient viscous responses, respectively [27]. According to Ivins et al. [27], SBM and EBM have similarities if the respective parameters are properly adjusted. Performing simple experiments involving deformations of an EBM half-space, Ivins et al. [28] point out that purely elastic models are not appropriate to account for deformations from inter-annual time scale, and Maxwell models may lead to long-term viscosity of the low mantle. Thus, they favor the use of transient rheologies. Transient rheologies have already been discussed by Yuen et al. [29] and Peltier et al. [30] in the framework of GIA. They concluded that transient rheologies are not crucial for understanding GIA, particularly in the North American region. Sabadini et al. [31] discussed the effect of transient rheologies with respect to the viscosity of the lower mantle. They found that transient rheologies can achieve similar results but with a different viscosity profile than that with Maxwell. These previous studies were mainly focused on the deformations induced by the Pleistocene deglaciation. Including LIA and present ice-mass changes in Greenland, Paxman et al. [32] obtained similar results to those of Ivins et al. [28]. The transient rheologies could be used to unify low and high mantle viscosities estimated from decadal to centennial and millennial surface-mass changes. Simon et al. [33] showed that SBM allows for a better explanation of the rapid changes of the near-field postglacial sea level than the Maxwell rheology. Based on Ivins et al. [34], using SBM argues that deformation estimated by the EBM does not show complex temporal changes given gradual surface-mass changes. Michel and Boy [35] highlighted the importance of the anelasticity of the Earth mantle in estimating the deformations due to present melts, especially for low-degree deformations.

The Andrade rheology is also a transient rheology frequently employed in astronomical and planetary studies to account for energy dissipation [36–38]. This rheology has a steady-state phase represented by a Maxwell element, such as SBM and EBM, and a transient phase driven by a power-law function of time [39]. Gevorgyan et al. [38] indicated that it is possible to interpret the non-Maxwell contribution of the Andrade rheology as a

continuum of Kelvin-Voigt elements added in series. Indeed, they approximated the Andrade rheology using 6 K-Voigt elements when studying Enceladus' energy dissipation due to libration. Yet, the Andrade rheology has not been employed to study GIA, and the SBM or EBM has not been used in Antarctica.

This paper aims at assessing the differences between using Maxwell, Burgers and Andrade rheologies when estimating geodetic parameters in response to GIA induced by short and long-term ice-mass change in Antarctica. It is not the goal of this paper to explain current observations. As mentioned above, the effects of lateral changes in the Earth's structure have been studied. Thus, we want to investigate the following questions: i) For a typical Earth structure, whether there is a significant difference in deformation due to past and present ice-mass changes using these three rheological methods. ii) How strong viscosity contrasts in the upper mantle affect these deformations. iii) How the predicted cumulative deformations and rates are affected by the three rheologies.

## 2. Modeling strategy

### 2.1. Formalism

To model the Earth's deformations and gravity changes in response to surface ice-mass changes, we use the gravito-viscoelasticity theory and Green's function formalism [13,40]. This formalism requires the computation of Love Numbers (LNs) introduced by Love (1909) [41]. Love Numbers are dimensionless numbers that reflect the inner structure of the Earth and relate the deformations and gravity changes of the Earth to the cause of the deformation [40,42,43]. Ice changes result from a change in the ice-mass distribution at the Earth's surface, representing a surface loading. In the spherical harmonic formalism, a surface-mass distribution ( $\sigma_n$ ) of harmonic degree ( $n$ ) induces a radial ( $u_n$ ) and tangential ( $v_n$ ) displacement of the surface as well as a change in the gravity potential ( $\phi_n$ ) of the same degree. Loading Love Numbers (LLNs)  $h'_n$ ,  $l'_n$  and  $k'_n$ , describing the capability of the Earth to deform when submitted to a unit surface forcing, are related to displacements and gravity changes by the following relations [44]:

$$u_n = \frac{h'_n}{\rho_e} \frac{3}{2n+1} \sigma_n \quad (1)$$

$$v_n = \frac{l'_n}{\rho_e} \frac{3}{2n+1} \sigma_n \quad (2)$$

$$\phi_n = \frac{1+k'_n}{\rho_e} \frac{3\gamma}{2n+1} \sigma_n \quad (3)$$

where  $\rho_e$  is the average density of the Earth and  $\gamma$  is the surface gravity.

Several methods have been implemented to compute LLNs, like the normal mode approach [13,45] and the propagator approach [46]. With the ALMA (plAnetary Love nuMbers cAlculator) software, Melini et al. [47] introduced an original strategy to integrate the gravito-viscoelasticity equations numerically. ALMA can rapidly and accurately compute the LLNs for a spherically symmetric, non-rotating, incompressible and self-gravitating Earth model, as well as the Heaviside loading function. Using the Post-Widder formula, it employs a numerical Laplace inversion of the Love number equations [48–50]. LLNs computed using ALMA are close to the ones calculated using other approaches [51]. More explanations of the method are shown in Spada (2003) [44] as well as Spada and Boschi (2006) [52].

## 2.2. Earth's radial structure

We use two models for the Earth's inner structure derived from the Preliminary Reference Earth Model (PREM) [53]. The models have a different number of layers. For each layer, rigidity and density are averaged from the PREM radial structure. Since we select the ICE-6G\_C (VM5a) deglaciation model [25,54] for investigating the effects of rheologies on GIA estimates, the associated VM5a viscosity profile is used. The VM5a model includes a 100 km thick elastic lithosphere, a viscosity of the upper mantle  $\eta_{UM} = 0.5 \times 10^{21}$  Pa·s, a 530 km shallow lower mantle with a viscosity  $\eta_{LM1} = 1.6 \times 10^{21}$  Pa·s, and a deep lower mantle with a viscosity  $\eta_{LM2} = 3.1 \times 10^{21}$  Pa·s. We also use a modified version of this viscosity profile to account for recently published results in important ice-melting areas [17,19,20]. This profile, called VM5am, divides the upper mantle into two viscoelastic layers. The shallow upper mantle is 120 km thick with a viscosity  $\eta_{SUM} = 1.0 \times 10^{18}$  Pa·s, assuring a large viscosity contrast as suggested by previously cited studies, while the deep upper mantle has the same properties as VM5a. The parameters of these models are described in Fig. 1.

## 2.3. Rheological law

Describing quasi-instantaneous and prolonged surface displacements or gravity changes is usually realized by invoking a viscoelastic body. The most often used viscoelastic rheology in GIA studies is the Maxwell law [13,55]. A body driven by such a law behaves elastically instantaneously and is characterized by a viscous steady-state behavior for longer loading. For a Maxwell body submitted to a Heaviside loading, the creep compliance function JM describes the strain variations under a step function of stress [39]. Following Ivins et al. [27], we obtain the normalized compliance  $\Psi_M$ . The normalizing factor is  $\frac{\sigma_0}{2\mu}$ , where  $\sigma_0$  is the initial loading stress and  $\mu$  is the rigidity. The normalized compliance function is given as [36]:

$$\Psi_M(t) = \left(1 + \frac{t}{\tau_M}\right)H(t) \quad (4)$$

where  $t$  is the time,  $H(t)$  is the Heaviside function,  $\tau_M$  is the Maxwell time with  $\tau_M = \frac{\eta}{\mu}$ , and  $\eta$  is the viscosity. To illustrate the strain variations of a Maxwell medium, we consider a stress function representing an unloading and a loading phase at  $t = 20$  yrs and  $t = 70$  yrs, respectively. Assuming that  $\mu = 10^{11}$  Pa·s and  $\eta = 10^{21}$  Pa·s, Fig. 2 shows the synchronous unloading phase and the elastic deformation followed by the steady-state deformation and the non-recoverable strain after the loading phase.

A Burgers viscoelastic body can be described as a Maxwell body to which a Kelvin-Voigt element has been added, enabling a transient response. This transient response allows the stressed medium to gradually deform from the elastic response to the steady state behavior. It is often used to explain postseismic deformations [26,56]. To describe the transient phase, the Burgers law requires a second viscosity  $\eta'$  and a second rigidity  $\mu'$ . Then, the normalized creep compliance function for the Burgers rheology  $\Psi_B$  takes the following form [27]:

$$\Psi_B(t) = \left(1 + \frac{t}{\tau_M} + \frac{\mu}{\mu'} \left(1 + e^{-\frac{t}{\tau'}}\right)\right)H(t) \quad (5)$$

where  $\tau' = \frac{\eta'}{\mu'}$ . Considering the same unloading and loading history, Fig. 2a and b shows the effects of  $\frac{\eta'}{\eta}$  and  $\frac{\mu'}{\mu}$  on  $\Psi_B$ , respectively. Fig. 2a

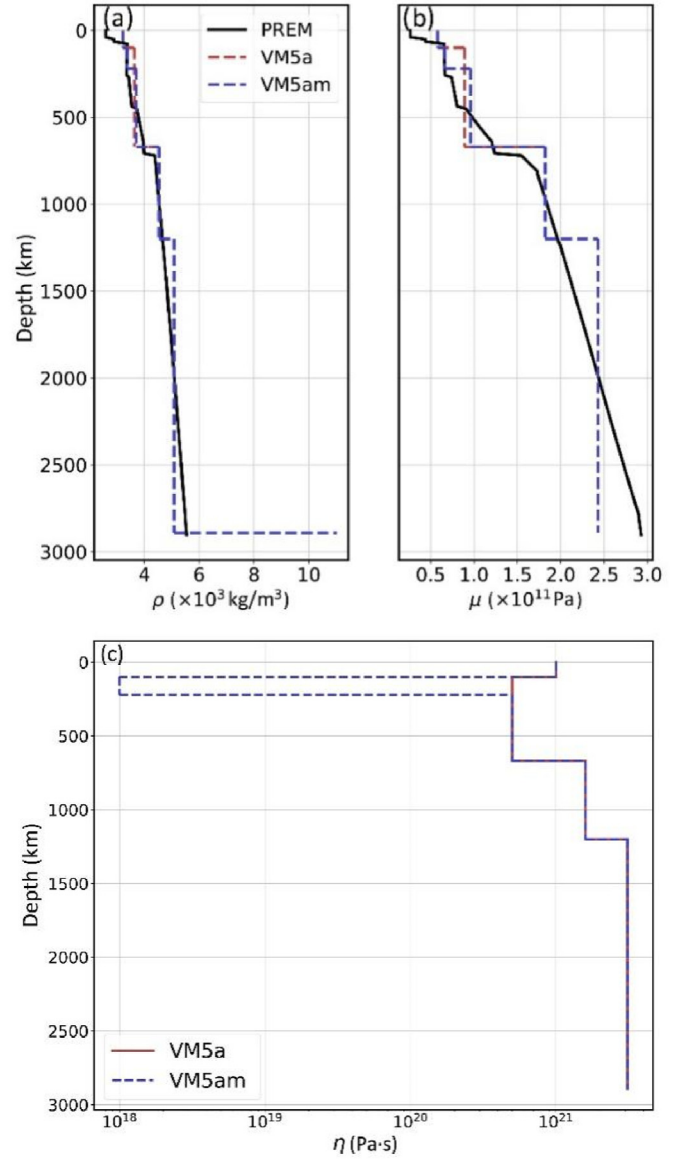
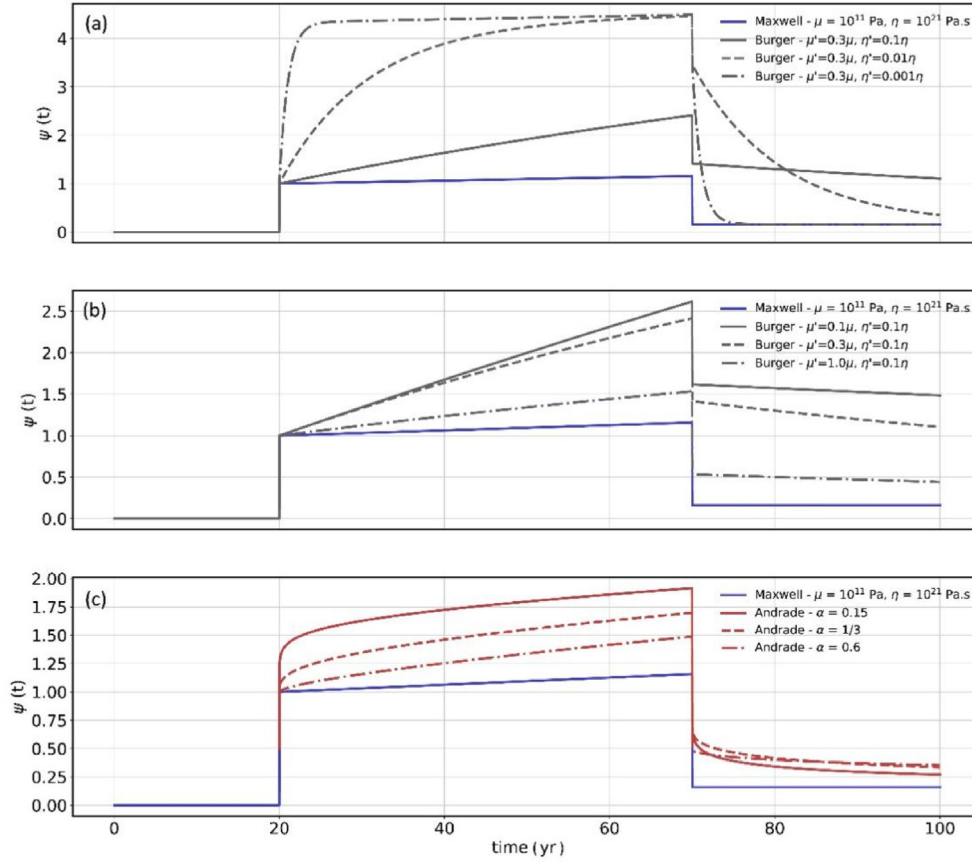


Fig. 1. (a) Density, (b) rigidity and (c) viscosity profiles of the Earth models VM5a and VM5am.

shows that the  $\frac{\eta'}{\eta}$  controls the timing of the transient response, with a lower ratio greatly shortening its duration. Fig. 2b shows that the  $\frac{\mu'}{\mu}$  controls the amplitude of the response, with a lower ratio leading to a larger response. To estimate postseismic rebound, it is common to use  $\frac{\eta'}{\eta} \in [0.01, 0.1]$  and  $\frac{\mu'}{\mu} \in [0.1, 1]$ .

The Andrade rheology is an extension of the Maxwell rheology by adding a damping term to the creep compliance function represented as a power law of time. A discussion of this model is introduced by Gevorgyan et al. [38]. It is often used to model tidal deformations, accounting for the energy dissipation of telluric bodies. We assume that the relaxation time (i.e., the time required for a body to reach 63% of the full deformation) is the same for both the Andrade and Maxwell rheologies [36]. That time is written as  $\tau_M = \tau_A = \frac{\eta}{\mu}$ . The normalized creep compliance function for the Andrade rheology ( $\Psi_A$ ) is [36]:



**Fig. 2.** Deformations over time due to unloading at  $t = 20$  yrs and loading at  $t = 70$  yrs for the Maxwell, Andrade and Burgers rheologies with  $\sigma_0 = 1$  Pa. The effects of (a) the  $\frac{\eta'}{\eta}$  ratio, (b) the  $\frac{\mu'}{\mu}$  ratio, and (c) the  $\alpha$  parameter.

$$\Psi_A(t) = \left( 1 + \frac{t}{\tau_M} + \left( \frac{t}{\tau_M} \right)^\alpha \right) H(t) \quad (6)$$

where  $\alpha$  is a physical parameter representing the transient response [36,57], ranging as  $\alpha \in [0.15, 0.6]$ . Referring to the same stress history, Fig. 2c shows the impact of that parameter. Similarly to the  $\frac{\eta'}{\eta}$  ratio,  $\alpha$  acts on the duration of the transient response and its amplitude.  $\alpha$  is usually taken between 0.33 and 0.5 [37,47,58,59], mainly as 1/3. Using the same parameters defining the Maxwell element, the SBM and Andrade rheology lead to the largest strain compared to the purely Maxwell medium.

## 2.4. Sensitivity of LLNs to rheologies and viscosity profiles

### 2.4.1. Variations in LLNs due to rheological parameters

The Andrade and Burgers rheologies require more parameters than the ones used to describe the Maxwell rheology. The effect of those parameters on LLNs is investigated. We compute the Heaviside LLNs one year after the loading for the Earth model VM5a with Burgers and Andrade rheologies and the harmonic degrees ranging from 2 to 400.

Fig. 3 shows the LLNs with an SBM having  $\frac{\mu'}{\mu} = 0.3$  [26,56,60] and  $\frac{\eta'}{\eta}$  in  $\{0.001, 0.01, 0.1\}$  and an Andrade rheology with  $\alpha$  in  $\{0.15, 0.33, 0.45, 0.6\}$ . We consider  $\frac{\eta'}{\eta} = 0.001$ , corresponding to a transient relaxation time 300 shorter than the Maxwell time, to illustrate a relatively rapid transient response of an SBM (Fig. 2).

Except for  $\frac{\eta'}{\eta} = 0.001$ , both rheologies show similar variations of LLN as a function of increasing degrees. The largest differences are observed for degrees lower than 250 for both rheologies. Beyond 300, there is no notable effect if we change the ratio  $\frac{\eta'}{\eta}$  and the parameter  $\alpha$ . This indicates that the transient response can impact LLNs for degrees lower than 200 or equivalently to the deformation of a wavelength larger than 200 km.

Few differences are observed using a ratio of 0.01 and 0.1 in the case of the Burgers rheology. The greatest differences are obtained with a ratio of 0.01, 0.1, or 0.001. Further, we keep the ratio of 0.1 [26,56,60] as a reference to estimate the impact of the Burgers rheology on GIA modeling.

There are tiny differences in the LLNs with  $\alpha$  ranging from 0.33 to 0.6. However, discrepancies are obtained with  $\alpha = 0.15$  at the level of the differences in the SBM between  $\frac{\eta'}{\eta} = 0.01$  and 0.1. Thus, the LLNs are weakly sensitive to a change in this parameter. Given that, we use the classical value of  $\alpha = 1/3$  for the rest of this study.

### 2.4.2. Effects of the Earth model on the LLNs

To investigate the effect of the rheologies on the time response of the Earth to loading, we compute LLNs 1, 10, 100, 1,000, and 10,000 years after the loading for degrees up to 250 using the six Earth models. Results with the elastic responses are shown in Figs. 4–6.

LLNs obtained with the VM5a profile deviate from the elastic response ten years after the loading for the Andrade and Burgers rheologies and one hundred years after the loading for the Maxwell rheology. For VM5am, the differences are notable as

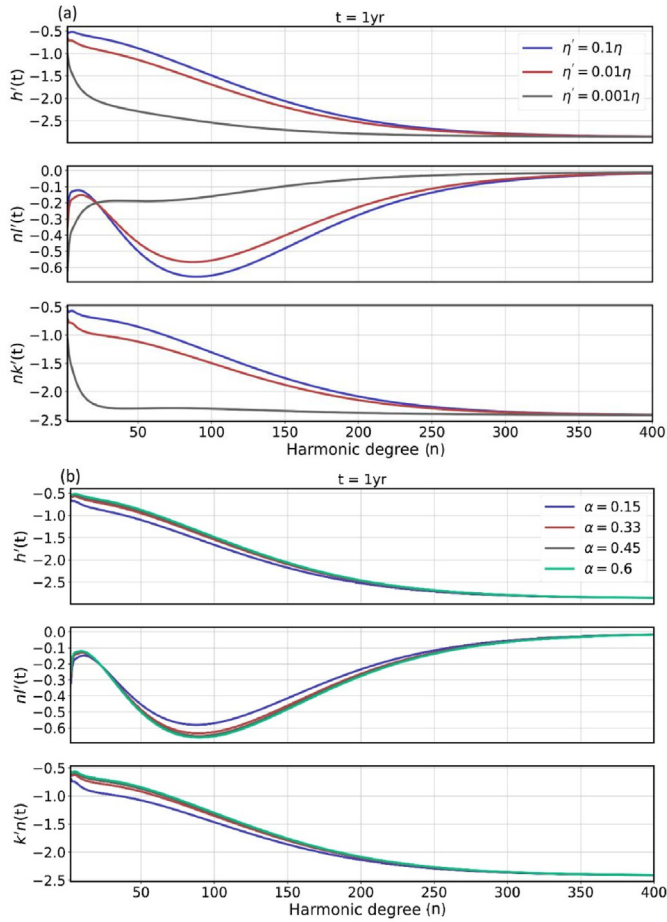


**Fig. 3.** LLNs computed using the Earth model VM5a with the (a) Burgers and (b) Andrade rheologies for  $\frac{\eta}{\eta_0}$  and  $\alpha$  one year after loading.

early as one year after the loading for all the rheologies. All rheologies and Earth's viscosity profiles lead to  $h'_n$  and  $k'_n$  that converge to the elastic limit for degrees larger than 225 and 150 one and ten thousand years after the loading. For degrees larger than 200, the discrepancies in LLNs concerning the Maxwell rheology for any rheology and Earth's structure are lower than 2.5%. This means that for wavelengths smaller than 200 km, the time response of our Earth models is similar and close to the elastic one.

LLNs calculated for the VM5a model show notable differences for decennial to millennial time scales and harmonic degrees ranging between 10 and 150. Discrepancies with respect to the Maxwell rheology range between 10% and 45% for the Andrade rheology and between 5% and 140% for the SBM. The largest effect induced by different rheologies is obtained one hundred years after the loading for both rheologies. After ten thousand years, the differences in LLNs for both profiles and all rheologies are lower than 1.8%, which indicates that the rheologies do not affect LLNs ten thousand years after the loading for the considered Earth's structure.

LLNs computed for the VM5am models show a larger amplitude depending on the harmonic degree than that calculated for VM5a models. While the discrepancies between rheologies are important one year after the loading, they rapidly reduce as early as ten years after the loading and tend to zero one thousand years after the loading. Discrepancies between LLNs from VM5am and VM5a models are reduced to less than 1% ten thousand years after the

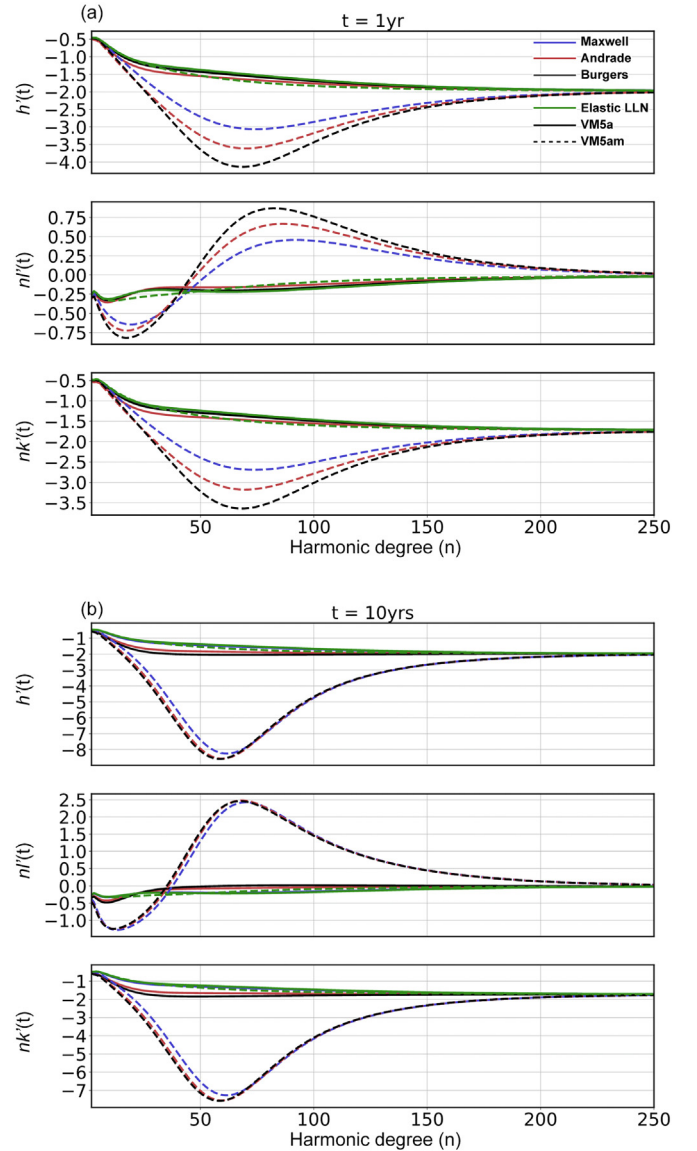


**Fig. 4.** LLNs computed for VM5a and VM5am Earth models using Maxwell (blue), Andrade (red) and Burgers (black) rheologies (a) one year and (b) ten years after the loading. The green curves show the elastic LLNs of the VM5a (solid) and VM5am (dashed) models.

loading. As expected, this implies that VM5am models are more sensitive to changes occurring at smaller spatial scales from annual to centennial time scales.

For VM5am models, the greatest effects induced by different rheologies are observed one year after loading for LLNs with harmonic degrees between 50 and 100. For VM5a models, it is rather one hundred years after loading for LLNs with harmonic degrees lower than 75. Besides, VM5am models lead to larger LLNs than VM5a models for a time scale lower than ten thousand years. These results indicate that a large viscosity contrast in the upper mantle leads to greater discrepancies in the viscous response and larger differences between rheologies from annual to centennial time scales. This implies that surface-mass changes occurring a few decades to centuries ago, such as during the LIA [18,19], might lead to different present Earth deformation depending on the rheology. Besides, given the different time responses depending on the viscosity structure and the rheology,

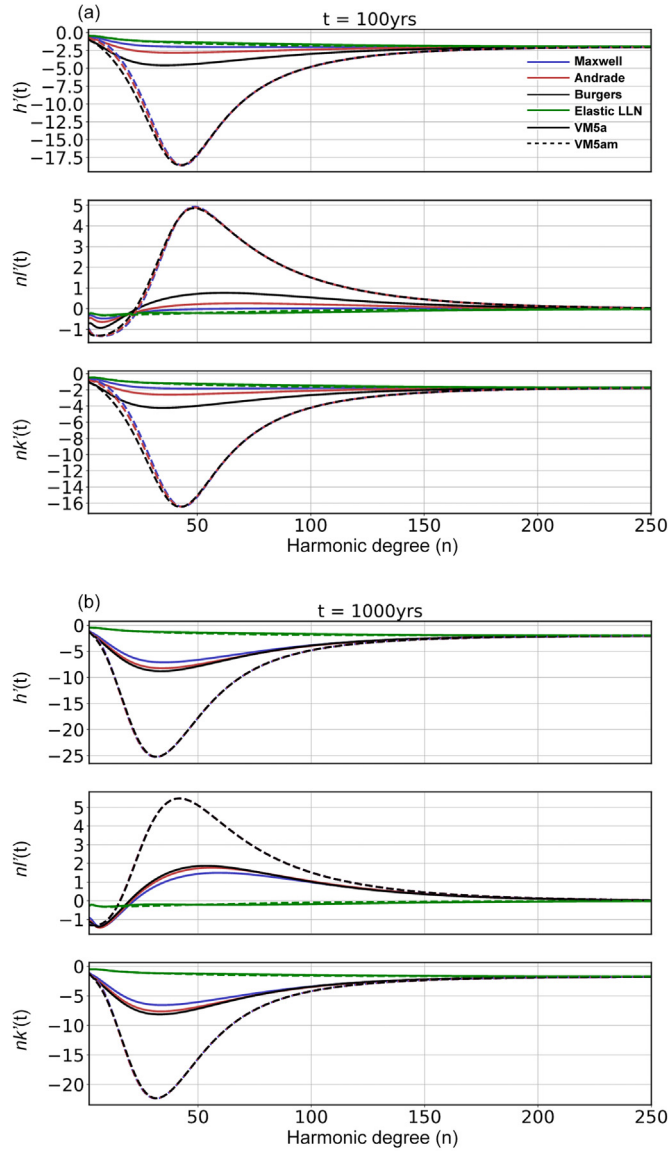


**Fig. 5.** LLNs computed for VM5a and VM5am Earth models using Maxwell (blue), Andrade (red) and Burgers (black) rheologies (a) 100 years and (b) 1000 years after the loading. The green curves show the elastic LLNs of the VM5a (solid) and VM5am (dashed) models.

the analysis of LLNs suggests that estimates of relative sea level (RSL) and paleo-shoreline changes might also be affected [33,61,62]. Next, we use the LLNs for these six Earth models to estimate displacements and gravity changes resulting from the past and present ice-mass changes.

### 3. Response to ice-mass change in Antarctica

#### 3.1. Predicting the deformation

The LLNs in section 2 are adopted to estimate the deformation induced by ice-mass changes at the surface of the Earth using the Green's function formalism. The Green's functions characterize the impulse response of the Earth to a point-mass excitation. The LLNs in section 2.3 are used to compute Green's functions for the surface radial displacement ( $G_{ur}$ ) and the surface gravity disturbance ( $G_g$ ). They are defined as [13,40]:

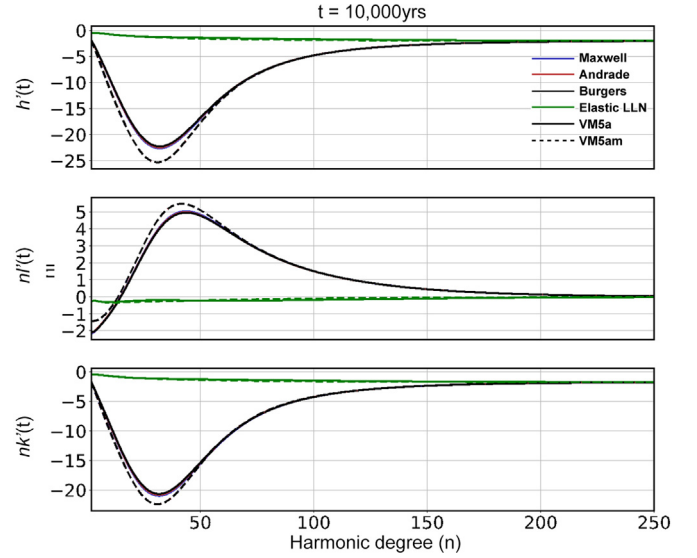


**Fig. 6.** LLNs computed for VM5a and VM5am Earth models using Maxwell (blue), Andrade (red) and Burgers (black) rheologies 10,000 years after the loading. The green curves show the elastic LLNs of the VM5a (solid) and VM5am (dashed) models.

$$G_{ur}(\psi, t) = \frac{\Gamma}{\gamma a} \sum_{n=0}^{\infty} h'_n(t) P_n(\cos \psi) \quad (7)$$

$$G_g(\psi, t) = -\frac{\Gamma}{a^2} \sum_{n=0}^{\infty} n \left( 1 - \frac{n+1}{n} k'_n(t) + \frac{2}{n} h'_n(t) \right) P_n(\cos \psi) \quad (8)$$

where  $t$  is time,  $P_n$  is the Legendre polynomial,  $\psi$  is the angular distance between the point estimating the deformation and the source of the deformation,  $\Gamma$  is the universal gravitational constant, and  $a$  is the Earth's mean radius. The source of the deformation is usually not a point mass but a surface distribution of mass  $\sigma_L$  that varies with time at the surface of the Earth. Then the Green's functions are convoluted with the surface-mass distribution to compute Green's functions for the surface radial displacement ( $G_{ur}$ ) and the surface gravity disturbance ( $G_g$ ). The convolution can be written as:

$$X(\theta, \phi, t) = \iint_{\Omega} \int_{-\infty}^t G_X(\psi, t-t') \sigma_L(\theta', \phi', t') dt' d\Omega \quad (9)$$

where  $\Omega$  is the total area covered by the surface-mass distribution,  $d\Omega = a^2 \sin\theta' d\theta' d\phi'$  is the elementary area,  $X$  is  $ur$  or  $g$ . We use the open-source TABOO software from Spada [44] to perform the convolution (9). The original version of TABOO allows the computation of the surface displacements and the geoid changes of a spherically symmetric, non-rotating, incompressible, self-gravitating, and Maxwell Earth model induced by a load. We modified TABOO to compute the surface gravity changes [19] and input LLNs from ALMA. The native spherical harmonics expansion of the ocean redistribution function in TABOO is limited to degree 180. However, Figs. 4–6 show that there would be little differences in the modeling for degrees beyond 180, with expected discrepancies in LLNs no larger than 4%. Therefore, we limit the modeling to that harmonic degree.

#### 3.2. Pleistocene deglaciation

The past ice history in Antarctica is complex and not entirely understood due to the lack of observations, specifically observations of near-field paleo-shoreline evolution. Indeed, far-field

observations of paleo-shoreline evolution help to constrain the amount of ice, while near-field observations also provide constraints on the timing of ice-mass changes [61,62]. In Antarctica, paleo-shorelines are not available, which makes it difficult to properly estimate the history of the ice sheet during the Pleistocene. Therefore, it is possible to compare observations of present displacement and gravity rates with estimates derived primarily through the Maxwell Earth model. This section assesses the effect of the three rheologies (section 2.1) on GIA deformation resulting from the Pleistocene deglaciation in Antarctica.

To describe the ice-mass change history of the AIS during the Pleistocene, we use the model ICE-6G\_C (VM5a) [25,54]. The geometry of ICE-6G\_C (VM5a) is used in SELEN4 [63]. Ice-mass variations are described for each former iced area, approximated by 3,046 caps of  $0.61^\circ$  radius, from 26 kyrs ago to the present, using a time history of 500-year time steps. Even though the conservation of mass is implemented in TABOO, it was not designed to account for sea level changes induced by ice-mass changes. As SELEN4 integrates the sea level equation, we use SELEN4 to estimate the effect of sea level changes on deformations in Antarctica and compare predicted current radial displacement rates from TABOO with that from SELEN4 for ICE-6G\_C (VM5a) using the same Maxwell Earth model (VM5a). Considering sea level changes, the uplift rate in Antarctica would increase by 15%.

Fig. 7 shows the present radial displacement and gravity variation rates in Antarctica induced by the Pleistocene deglaciation estimated using the VM5a viscosity profile with a Maxwell

rheology. The pattern of the deformation rates is similar to that estimated by Argus et al. [54]. The largest deformations are mainly located in West Antarctica and South of the Antarctic peninsula. Fig. 7 c and d show the differences in radial displacement rates when using Andrade and Maxwell rheologies and using Burgers and Maxwell rheologies, respectively. The largest differences are located in West Antarctica and the Antarctic peninsula, where the largest geodetic rates are predicted (Fig. 7). Employing the Andrade rheology to model the present deformations due to the Pleistocene deglaciation leads to rates mainly lower than that obtained by the Maxwell rheology. Differences in uplift rates reach up to 0.5 mm/yr under the Ronne-Filchner ice shelf. The Burgers rheology leads to slightly larger and lower rates than the Maxwell rheology in East and West Antarctica, respectively. The largest difference is about  $\pm 0.2$  mm/yr.

To investigate the effect of viscosity structure and rheological laws on paleo-shoreline predictions, Fig. 8 shows the cumulative radial displacement ( $75^\circ\text{S}$  and  $63^\circ\text{W}$ ) during the last 26 kyrs computed using VM5a and VM5am Earth models. Adding a low-viscosity layer in the upper mantle directly impacts the total vertical uplift. Indeed, a 26 kyr-cumulated uplift derived using VM5am models is 40 m larger than that derived using VM5a models. For both VM5a and VM5am models, using Burgers and Andrade rheologies results in larger cumulative displacement than using Maxwell rheology, up to 1 m (VM5am) and 4 m (VM5a) after 26 kyrs (Fig. 8 c). A more detailed analysis (Fig. 8 b) shows that from 26 to 14.5 kyrs ago, the six Earth models led to very similar radial

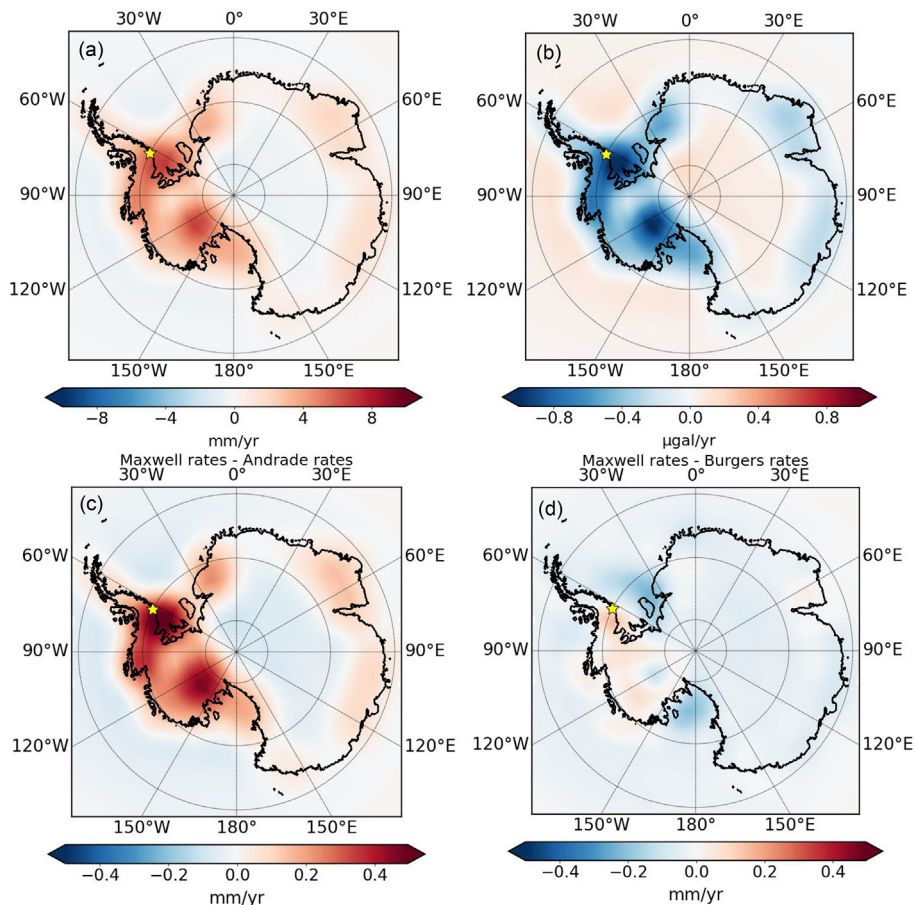
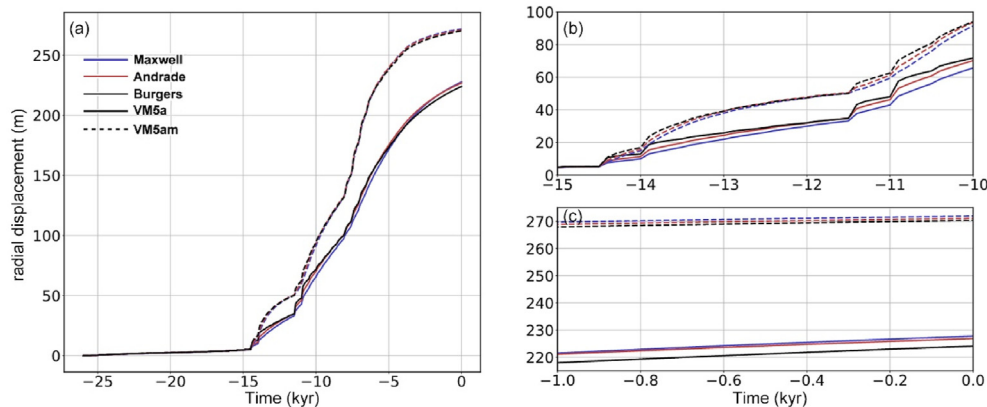


Fig. 7. (a) Present radial displacement and (b) gravity variation rates in Antarctica induced by the Pleistocene deglaciation estimated by the ICE-6G\_C (VM5a) deglaciation model and the VM5a viscosity profile, using a Maxwell rheology. Differences between present radial displacement rates estimated (c) using Maxwell and Andrade rheologies and (d) using Maxwell and Burgers rheologies due to the Pleistocene deglaciation in Antarctica. The yellow star indicates the estimated location of the time series in Fig. 8.



**Fig. 8.** Cumulative radial displacement during (a) the last 26 kyr estimated by ICE-6G\_C (VM5a) model using VM5a and VM5am Earth models. The observer is located on the shore of the Antarctic peninsula as shown in Fig. 7. As the same as (a), (b) is at the beginning of the melting of the AIS, and (c) is the last one kyr before the present.

displacements. Discrepancies in radial displacement between rheologies range from 5 to 20 cm, with Burgers providing the largest. During this time interval, the Northern Hemisphere is subject to essential mass changes while the AIS remains almost stable [25,54], which suggests that the models are not significantly sensitive to far-field mass changes. The AIS began to lose mass about 14.5 kyr ago, as indicated by the uplift of a few meters in Fig. 8b. Similar uplifts were observed at 11.5 and 11 kyr ago. These events represent a large change in relative sea level [64,65]. Fig. 8 illustrates that the viscosity structure and the rheologies significantly impact the timing of the deformations. The transient response of Burgers and Andrade rheologies leads to larger deformation during the first few centuries after deglaciation. Different rheologies do not result in different Earth responses at longer time scales. Consequently, deglaciation models based on paleo-shoreline evolution and cumulative surface displacements should be impacted using a strong viscosity contrast in the upper mantle and different rheologies.

### 3.3. Recent ice-mass change

To consider the present mass changes in Antarctica, we use the variations of the ice sheet elevation between January 2002 and November 2017 derived by Schröder et al. [67] from satellite altimetry. The glaciers showing the greatest elevation variation are the Thwaites Glacier and Pine Island Glacier (PIG), with elevation variation exceeding 20 cm/yr [66,67]. We model the ice-mass variation by covering the Antarctic surface with 1,784 ice caps of  $0.43^\circ$  of half amplitude. Caps located south of  $85^\circ\text{S}$  are excluded as little altimetry data is available for these latitudes due to the orbit geometry of satellites. We also exclude any cap with no thickness variation. The height variation associated with each cap is averaged from altimetry height changes. The yearly piecewise constant phases are used to describe the temporal variations of the AIS height that combined with the density ( $931\text{ kg/m}^3$ ) of pure ice as an upper boundary for the local mass changes [68]. This forms the present-day ice-mass change (PDIMC) model. The distribution of caps and the associated height change rates are shown in Fig. 9a.

Fig. 9b and c shows the vertical displacement and the gravity variation close to PIG (yellow star in Fig. 9c) for the six Earth models. The observer's location is chosen near PIG where the mass change is the largest over the studied time interval, which should result in the largest deformation. The purely elastic deformation (green curves in Fig. 9b and c) is similar in all Earth models and contributes the most to the cumulative vertical displacement using the VM5a model in 2017. It is less than 50 % of the total deformation

for the VM5am model. In VM5am models, the low viscosity layer within the upper mantle more than doubles the deformation.

Regarding the viscous deformation in 2017, Andrade and Burgers rheologies led to larger uplift and gravity change than the Maxwell rheology. The difference reaches about  $20\text{ mm}/3\text{ }\mu\text{gal}$  and about  $27\text{ mm}/4\text{ }\mu\text{gal}$  for VM5a and VM5am Earth models, respectively. Besides, for VM5a models, the Maxwell rheology induces neglectable viscous deformation compared to the elastic deformation [20]. After 2017, the ice mass stopped changing in the PDIMC model. The viscous response increases the discrepancies between deformations resulting from the three rheologies. The largest differences between vertical displacement and gravity variation are obtained using Maxwell and Burgers rheologies with the VM5a profile. They reach up to 100 mm and  $16.5\text{ }\mu\text{gal}$  in 2070.

To better understand the changes induced by different rheologies and the two viscosity profiles, the time-varying rate of the vertical displacement and the gravity variation are plotted in Fig. 10. VM5am models lead to rates more than five times that estimated using VM5a models, showing that the inclusion of a low viscosity layer within the upper mantle can help to reconcile geodetic rates derived from observations with model predictions [17,19,20]. An effect is noticeable when comparing the rates obtained from the three rheologies using VM5am. Indeed, using the Burgers rheology led to instantaneous rates that are 10 and 41 % larger than that from using Andrade and Maxwell rheologies in 2017. Discrepancies in rates derived using different rheologies are the largest when the ice mass stopped changing in 2017. They converge to reach similar values about 50 years later for VM5am models. This convergence takes more time for VM5a models, specifically between rates estimated using the Burgers rheology and those using the other two rheologies.

## 4. Discussion

### 4.1. About the relative sea level

Most of the recent Pleistocene deglaciation models, such as W12 [69], IJ05\_R2 [70], A13 [71], or ICE-6G\_C (VM5a) [25,54], use paleo-shoreline observations in Scandinavia and North America to constrain the deglaciation history. As these regions have constraints on far- and near-field observations, the deglaciation history is expected to be more accurately estimated [61,62]. These models employ a Maxwell viscoelastic Earth to estimate the timing and amount of ice involved in the deglaciation. In sections 3.2 and 3.3,

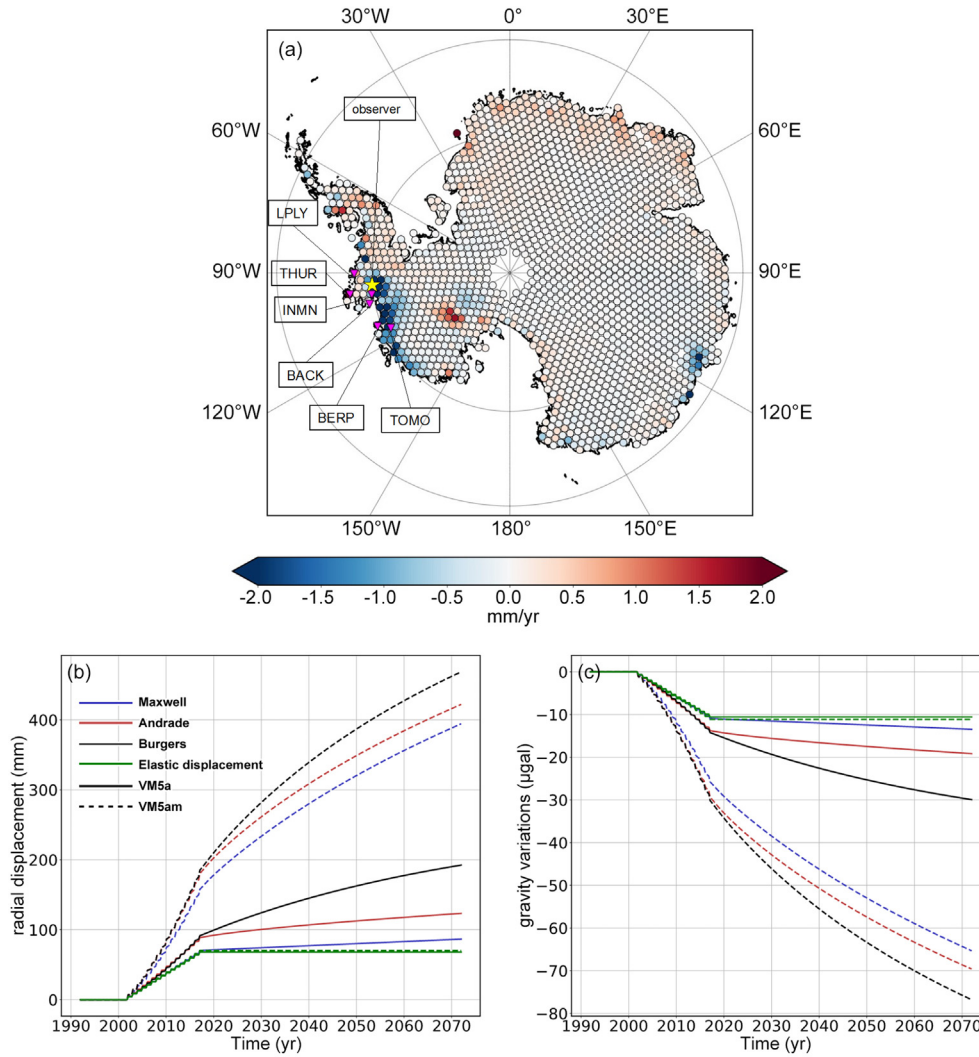


**Fig. 9.** (a) Thickness variation rates between 2002 and 2017 for the PDIMC model of the AIS. Pink triangles show the locations of the GPS stations used in Barletta et al. (2018) [20]. The yellow star shows the location where (b) vertical displacement and (c) gravity variations are estimated using the Maxwell, Andrade and Burgers rheologies. The deglaciation started in 2002 and ended in 2017. The green lines show the purely elastic response for the VM5a and the VM5am Earth models.

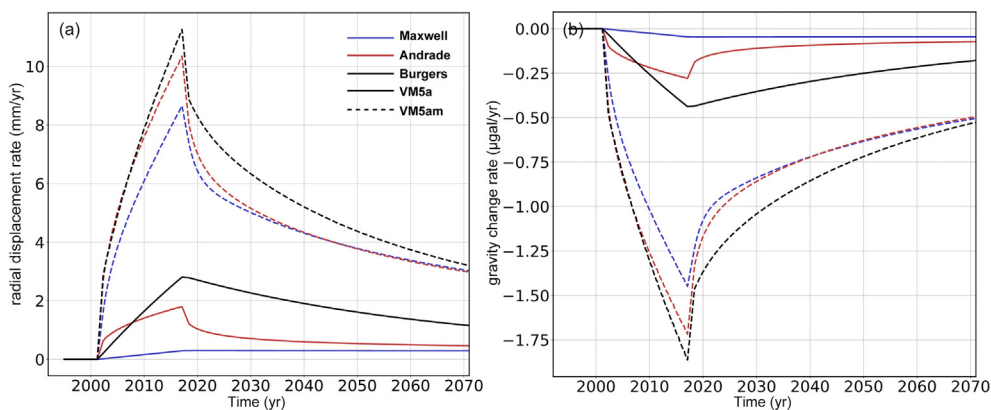


**Fig. 10.** Time-varying rates of (a) the viscous radial displacement and (b) gravity variation estimated near PIG (yellow star in Fig. 9a).

we present the accumulated radial displacement for the ICE-6G\_C (VM5a) and PDIMC models. The viscosity profiles have the largest impact on the accumulated radial displacement, leading to an increase of more than 40 m. Rheologies with a transient response

have a lower effect on displacement estimation, increasing the decennial to centennial time scales up to 10 m for the ICE-6G\_C (VM5a) model. Similar results are obtained for the PDIMC model, with differences in displacement ranging up to 20 cm. These results

show that rheologies have an impact on constraining near-field mass changes. Consequently, using different rheologies to model past ice-mass changes from paleo-shoreline observations should lead to varying chronologies of mass evolution. Therefore, it is expected that changing the rheology is likely to have a notable effect when modeling the northern hemisphere deglaciations where the paleo-shorelines are available, meeting the conclusions by Simon et al. [33].

#### 4.2. About the upper mantle viscosity

Nield et al. (2014) [17] found that the Earth model that better explains GNSS data in the Antarctic Peninsula has a lithosphere thickness of 140 km and an upper mantle viscosity ranging between  $6 \times 10^{17}$  and  $2 \times 10^{18}$  Pa·s. Working on the Fleming glacier in the Antarctic peninsula, Zhao et al. [72] suggested a viscosity for the upper mantle between  $10^{19}$  and  $10^{20}$  Pa·s, based on a multi-decadennial study of the ice-mass change. This discrepancy in the result could be explained by a timescale dependency on the upper mantle viscosity.

Other examples of upper mantle viscosities inferred from present-day ice-mass changes are found in Greenland and Svalbard. Mémin et al. [19] inferred the shallow upper mantle viscosity from gravity variation and vertical uplift observations induced by past (Pleistocene, LIA) and present ice-mass changes. They found that a viscosity ranging from 1.0 to  $5.5 \times 10^{18}$  Pa·s and a lithosphere thickness between 50 and 100 km can explain the observed geodetic rates. Similar results were recently obtained for the Greenland region by Paxman et al. (2023). According to Adhikari et al. [73], an estimation of the mantle viscosity is inferred from sub-centennial mantle deformation and compared to GIA estimates in Greenland. These estimates are derived from GNSS observations. The upper mantle viscosity should at least be one order of magnitude below the value commonly found in GIA studies, with a viscosity ranging from 3 to  $11 \times 10^{19}$  Pa·s. The study of Paxman et al. [32] on the timescale-dependent apparent viscosity of the upper mantle in Greenland also agrees with these results. They found that the apparent viscosity of the upper mantle depends on the timescale, with a viscosity of  $10^{18}$  Pa·s for the decennial periods and  $10^{19}$  Pa·s for the centennial periods at a depth of 200 km. The upper mantle viscosity keeps a stable value of about  $6 \times 10^{20}$  Pa·s for multi-millennial periods and above. Considering a Maxwell viscoelastic Earth, these estimations are obtained to account for the current bedrock uplift rates due to the present melting. Several studies based on GNSS and satellite altimetry observations show a timescale dependency on the viscosity of the upper mantle. As shown in section 2.1, the Andrade and Burgers rheologies have a short-term transient response with viscosities up to 2 orders of magnitude lower than the millennial time scale. Using rheologies with a transient response should be investigated to explain these observations.

Section 3.3 highlights differences in the estimated uplift rates, especially between Burgers and Maxwell rheologies for PDIMC models. The uplift and gravity variation rates derived using the Burgers rheology can be ten times larger than those estimated using the Maxwell rheology. Similarly, with the Andrade rheology, we obtain rates up to 4.5 times larger than that derived using the Maxwell rheology. Results from sections 3.2 and 3.3 show that adding a low-viscosity layer increases the PDIMC deformation rates but decreases the Pleistocene rates. These results indicate that the Earth needs to be less viscous for short-term mass changes and more viscous for long-term deglaciation periods. This can be achieved using transient rheologies such as Andrade or Burgers, with more tuning of the parameters controlling the short-term transient response of the Earth.

## 5. Conclusion

This study computes the LLNs for six Earth models involving the viscoelastic rheologies of Maxwell, Andrade, and Burgers and two viscosity profiles: the VM5a [25,54] and a modified version VM5am that includes a 120 km-thick layer in the upper mantle with a viscosity of about three orders of magnitude lower. The different responses are observed using the three rheologies mainly for loading wavelengths larger than 200 km. Besides, the large viscosity contrast in the upper mantle amplifies the discrepancies in the viscous responses from annual to centennial time scales.

Then, the radial displacement and surface gravity disturbances are estimated from the ICE-6G\_C (VM5a) past deglaciation model and the PDIMC model derived from satellite altimetry. We compare the predicted rates from the six Earth models to assess their effect on the amplitude and the chronology of the geodetic variations. The largest impact on GIA-induced geodetic parameters is due to the low viscosity layer in the upper mantle. This layer increases the total displacement caused by the Pleistocene deglaciation by up to about 40 m and the PDIMC by up to 240 mm. Using the ICE-6G\_C (VM5a) model, the Burgers and Andrade rheologies lead to a difference up to 10 m in radial displacement during the first few centuries after ice-mass changes.

Introducing a strong viscosity contrast in the upper mantle can lead to PDIMC-induced geodetic rates more than five times larger than those without PDIMC. In the low-viscosity layer, the displacement and gravity variability induced by Burgers and Andrade rheologies are larger than those induced by Maxwell rheology, up to 41% and 31%, respectively.

Comparing the model with the observed vertical displacement rates gives insight into how considering different rheologies and viscosity structures can help reduce errors. Assuming a low-viscosity layer within the upper mantle and using both Burgers and Andrade rheologies also reduce the misfit. Several other studies have shown that the upper mantle viscosity is likely to be time-dependent. Using a transient rheology, including a short-term viscous response to the Earth, should improve GIA modeling by unifying the effects induced by past and present ice-mass changes within a single rheological law.

## Conflicts of interest

The authors declare that there is no conflicts of interest.

## Acknowledgment

This work has been partly funded by the Centre National d'Etudes Spatiales (CNES) through the TOSCA program. We thank the Astrogeo team from Geoazur for their helpful feedback and exchanges. We also thank Giorgio Spada and Daniele Melini for providing freely the ALMA3 and TABOO softwares. We thank Giorgio Spada and an anonymous reviewer for their comments that greatly improve the first draft of this paper. All authors declare no conflicts of interest.

## References

- [1] IMBIE, Mass balance of the antarctic ice sheet from 1992 to 2017, *Nature* 558 (2018) 219–222, <https://doi.org/10.1038/s41586-018-0179-y>.
- [2] D.J. Wingham, A.J. Ridout, R. Scharroo, R.J. Arthern, C. Shum, Antarctic elevation change from 1992 to 1996, *Science* 282 (1998) 456–458, <https://doi.org/10.1126/science.282.5388.456>.
- [3] J. Wahr, I. Velicogna, Measurements of time-variable gravity show mass loss in antarctica, *Science* 311 (2006) 1754–1756, <https://doi.org/10.1126/science.1123785>.
- [4] I. Velicogna, Y. Mohajerani, G. A. F. Landerer, J. Mougnot, B. Noel, E. Rignot, T. Sutterley, M. Broeke, M. Wessem, D. Wiese, Continuity of ice sheet mass loss

- in Greenland and Antarctica from the GRACE and GRACE follow-on missions, *Geophys. Res. Lett.* 47 (2020), <https://doi.org/10.1029/2020gl087291>.
- [5] W. Peltier, Glacial-isostatic adjustment—ii. the inverse problem, *Geophys. J. Int.* 46 (1976) 669–705, <https://doi.org/10.1111/j.1365-246X.1976.tb01253.x>.
- [6] W.R. Peltier, J.T. Andrews, Glacial-isostatic adjustment—i. the forward problem, *Geophys. J. Int.* 46 (1976) 605–646, <https://doi.org/10.1111/j.1365-246X.1976.tb01251.x>.
- [7] B.D. Tapley, S. Bettadpur, M. Watkins, C. Reigber, The gravity recovery and climate experiment: mission overview and early results, *Geophys. Res. Lett.* 31 (2004), <https://doi.org/10.1029/2004GL019779>.
- [8] F.W. Landerer, F.M. Flechtner, H. Save, F.H. Webb, T. Bandikova, W.I. Bertiger, S.V. Bettadpur, S.H. Byun, C. Dahle, H. Dobslaw, et al., Extending the global mass change data record: grace follow-on instrument and science data performance, *Geophys. Res. Lett.* 47 (2020) e2020GL088306, <https://doi.org/10.1029/2020GL088306>.
- [9] T. Li, P. Wu, H. Wang, H. Steffen, N.S. Khan, S.E. Engelhart, M. Vacchi, T.A. Shaw, W.R. Peltier, B.P. Horton, Uncertainties of glacial isostatic adjustment model predictions in north America associated with 3d structure, *Geophys. Res. Lett.* 47 (2020) e2020GL087944, <https://doi.org/10.1029/2020GL087944>.
- [10] E. Powell, N. Gomez, C. Hay, K. Latychev, J.X. Mitrovica, Viscous effects in the solid earth response to modern antarctic ice mass flux: implications for geodetic studies of WAIS stability in a warming world, *J. Clim.* 33 (2020) 443–459, <https://doi.org/10.1175/jcli-d-19-0479.1>.
- [11] A. Hattori, Y. Aoyama, J. Okuno, K. Doi, GNSS observations of GIA-induced crustal deformation in lützow-holm bay, east Antarctica, *Geophys. Res. Lett.* 48 (2021), <https://doi.org/10.1029/2021gl093479>.
- [12] L. Cathles, Lower mantle viscosity inferred from post glacial adjustment of the ocean basin and Canada, in: *Trans. Am. Geophys. Union*, 1971, p. 353.
- [13] W. Peltier, The impulse response of a maxwell earth, *Rev. Geophys.* 12 (1974) 649–669, <https://doi.org/10.1029/RG012i004p00649>.
- [14] M. Tamisiea, J. Mitrovica, J. Davis, Grace gravity data constrain ancient ice geometries and continental dynamics over laurentia, *Science* 316 (2007) 881–883, <https://doi.org/10.1126/science.1137157>.
- [15] N.A. Haskell, The motion of a viscous fluid under a surface load, *Physics* 6 (1935) 265–269, <https://doi.org/10.1063/1.1745329>.
- [16] J.X. Mitrovica, Haskell [1935] revisited, *J. Geophys. Res. Solid Earth* 101 (1996) 555–569, <https://doi.org/10.1029/95JB03208>.
- [17] G.A. Nield, V.R. Barletta, A. Bordon, M.A. King, P.L. Whitehouse, P.J. Clarke, E. Domack, T.A. Scambos, E. Berthier, Rapid bedrock uplift in the antarctic peninsula explained by viscoelastic response to recent ice unloading, *Earth Planet. Sci. Lett.* 397 (2014) 32–41, <https://doi.org/10.1016/j.epsl.2014.04.019>.
- [18] J.M. Grove, *The little ice age*, Routledge, 2012.
- [19] A. Mémin, G. Spada, J.P. Boy, Y. Rogister, J. Hinderer, Decadal geodetic variations in ny-ålesund (svalbard): role of past and present ice-mass changes, *Geophys. J. Int.* 198 (2014) 285–297.
- [20] V.R. Barletta, M. Bevis, B.E. Smith, T. Wilson, A. Brown, A. Bordon, M. Willis, S.A. Khan, M. Rovira-Navarro, I. Dalziel, et al., Observed rapid bedrock uplift in amundsen sea embayment promotes ice-sheet stability, *Science* 360 (2018) 1335–1339, <https://doi.org/10.1126/science.aao1447>.
- [21] M.H. Ritzwoller, N.M. Shapiro, A.L. Levshin, G.M. Leahy, Crustal and upper mantle structure beneath Antarctica and surrounding oceans, *J. Geophys. Res. Solid Earth* 106 (2001) 30645–30670.
- [22] A. Morelli, S. Danesi, Seismological imaging of the antarctic continental lithosphere: a review, *Global Planet. Change* 42 (2004) 155–165, <https://doi.org/10.1016/j.gloplacha.2003.12.005>.
- [23] W. Van Der Wal, P.L. Whitehouse, E.J. Schrama, Effect of gia models with 3d composite mantle viscosity on grace mass balance estimates for Antarctica, *Earth Planet. Sci. Lett.* 414 (2015) 134–143, <https://doi.org/10.1016/j.epsl.2015.01.001>.
- [24] E.M. Powell, L. Pan, M.J. Hoggard, K. Latychev, N. Gomez, J. Austerermann, J.X. Mitrovica, The impact of 3-d earth structure on far-field sea level following interglacial west antarctic ice sheet collapse, *Quat. Sci. Rev.* 273 (2021) 107256, <https://doi.org/10.1016/j.quascirev.2021.107256>.
- [25] W.R. Peltier, D. Argus, R. Drummond, Space geodesy constraints ice age terminal deglaciation: the global ice-6g\_c (vm5a) model, *J. Geophys. Res. Solid Earth* 120 (2015) 450–487, <https://doi.org/10.1002/2014JB011176>.
- [26] F.F. Pollitz, Transient rheology of the uppermost mantle beneath the mojave desert, California, *Earth Planet. Sci. Lett.* 215 (2003) 89–104, [https://doi.org/10.1016/S0012-821X\(03\)00432-1](https://doi.org/10.1016/S0012-821X(03)00432-1).
- [27] E.R. Ivins, L. Caron, S. Adhikari, E. Larour, M. Scheinert, A linear viscoelasticity for decadal to centennial time scale mantle deformation, *Rep. Prog. Phys.* 83 (2020) 106801, <https://doi.org/10.1088/1361-6633/aba346>.
- [28] E.R. Ivins, L. Caron, S. Adhikari, Anthropocene isostatic adjustment on an anelastic mantle, *J. Geodesy* 97 (2023) 92, <https://doi.org/10.1007/s00190-023-01781-7>.
- [29] D.A. Yuen, R.C. Sabadini, P. Gasperini, E. Boschi, On transient rheology and glacial isostasy, *J. Geophys. Res. Solid Earth* 91 (1986) 11420–11438, <https://doi.org/10.1029/JB091iB11p11420>.
- [30] W. Peltier, D. Yuen, P. Wu, Postglacial rebound and transient rheology, *Geophys. Res. Lett.* 7 (1980) 733–736, <https://doi.org/10.1029/GL007i010p00733>.
- [31] R. Sabadini, D. Yuen, P. Gasperini, The effects of transient rheology on the interpretation of lower mantle viscosity, *Geophys. Res. Lett.* 12 (1985) 361–364, <https://doi.org/10.1029/GL012i006p00361>.
- [32] G.J.G. Paxman, H.C.P. Lau, J. Austerermann, B.K. Holtzman, C. Havlin, Inference of the timescale-dependent apparent viscosity structure in the upper mantle beneath Greenland, *AGU Adv.* 4 (2023), <https://doi.org/10.1029/2022av000751>.
- [33] K.M. Simon, R.E. Riva, T. Broerse, Identifying geographical patterns of transient deformation in the geological sea level record, *J. Geophys. Res. Solid Earth* 127 (2022) e2021JB023693, <https://doi.org/10.1029/2021JB023693>.
- [34] E.R. Ivins, L. Caron, S. Adhikari, E. Larour, Notes on a compressible extended burgers model of rheology, *Geophys. J. Int.* 228 (2022) 1975–1991, <https://doi.org/10.1093/gji/ggab452>.
- [35] A. Michel, J. Boy, Viscoelastic love numbers and long-period geophysical effects, *Geophys. J. Int.* 228 (2022) 1191–1212, <https://doi.org/10.1093/gji/ggab369>.
- [36] J.C. Castillo-Rogez, M. Efroimsky, V. Lainey, The tidal history of iapetus: spin dynamics in the light of a refined dissipation model, *J. Geophys. Res.: Planets* 116 (2011), <https://doi.org/10.1029/2010JE003664>.
- [37] M. Efroimsky, Tidal dissipation compared to seismic dissipation: in small bodies, earths, and super-earths, *Astrophys. J.* 746 (2012) 150, <https://doi.org/10.1088/0004-637X/746/2/150>.
- [38] Y. Gevorgyan, G. Boué, C. Ragazzo, L.S. Ruiz, A.C. Correia, Andrade rheology in time-domain. application to enceladus' dissipation of energy due to forced libration, *Icarus* 343 (2020) 113610, <https://doi.org/10.1016/j.icarus.2019.113610>.
- [39] U. Faul, I. Jackson, Transient creep and strain energy dissipation: an experimental perspective, *Annu. Rev. Earth Planet. Sci.* 43 (2015) 541–569, <https://doi.org/10.1146/annurev-earth-060313-054732>.
- [40] W.E. Farrell, Deformation of the earth by surface loads, *Rev. Geophys.* 10 (1972) 761, <https://doi.org/10.1029/rg010i003p00761>.
- [41] A.E.H. Love, The yielding of the earth to disturbing forces, *Proc. R. Soc. Lond. - Ser. A. Contain. Pap. a Math. Phys. Character* 82 (1909) 73–88, <https://doi.org/10.1098/rspa.1909.0008>.
- [42] I.M. Longman, A green's function for determining the deformation of the earth under surface mass loads: 1. theory, *J. Geophys. Res.* 67 (1962) 845–850, <https://doi.org/10.1029/jz067i002p00845>.
- [43] I.M. Longman, A green's function for determining the deformation of the earth under surface mass loads: 2. computations and numerical results, *J. Geophys. Res.* 68 (1963) 485–496, <https://doi.org/10.1029/jz068i002p00485>.
- [44] G. Spada, *The theory behind taboo*, Samizdat Press edn, 2003, p. 606.
- [45] L. Vermeersen, R. Sabadini, A new class of stratified viscoelastic models by analytical techniques, *Geophys. J. Int.* 129 (1997) 531–570, <https://doi.org/10.1111/j.1365-246X.1997.tb04492.x>.
- [46] R. Sabadini, D.A. Yuen, E. Boschi, Polar wandering and the forced responses of a rotating, multilayered, viscoelastic planet, *J. Geophys. Res. Solid Earth* 87 (1982) 2885–2903, <https://doi.org/10.1029/JB087iB04p02885>.
- [47] D. Melini, C. Saliby, G. Spada, On computing viscoelastic love numbers for general planetary models: the alma3 code, *Geophys. J. Int.* 231 (2022) 1502–1517, <https://doi.org/10.1093/gji/ggac263>.
- [48] E.L. Post, Generalized differentiation, *Trans. Am. Math. Soc.* 32 (1930) 723–781.
- [49] D.V. Widder, The inversion of the laplace integral and the related moment problem, *Trans. Am. Math. Soc.* 36 (1934) 107–200.
- [50] D.V. Widder, *The laplace transform*, vol. 6, 1941 [of Princeton Mathematical Series].
- [51] G. Spada, V.R. Barletta, V. Klemann, R. Riva, Z. Martinec, P. Gasperini, B. Lund, D. Wolf, L. Vermeersen, M. King, A benchmark study for glacial isostatic adjustment codes, *Geophys. J. Int.* 185 (2011) 106–132, <https://doi.org/10.1111/j.1365-246X.2011.04952.x>.
- [52] G. Spada, L. Boschi, Using the post-widder formula to compute the earth's viscoelastic love numbers, *Geophys. J. Int.* 166 (2006) 309–321, <https://doi.org/10.1111/j.1365-246X.2006.02995.x>.
- [53] A.M. Dziewonski, D.L. Anderson, Preliminary reference earth model, *Phys. Earth Planet. In.* 25 (1981) 297–356, [https://doi.org/10.1016/0031-9201\(81\)90046-7](https://doi.org/10.1016/0031-9201(81)90046-7).
- [54] D.F. Argus, W.R. Peltier, R. Drummond, A.W. Moore, The Antarctica component of postglacial rebound model ICE-6G\_C (VM5a) based on GPS positioning, exposure age dating of ice thicknesses, and relative sea level histories, *Geophys. J. Int.* 198 (2014) 537–563, <https://doi.org/10.1093/gji/ggu140>.
- [55] P. Wu, W.R. Peltier, Viscous gravitational relaxation, *Geophys. J. Int.* 70 (1982) 435–485, <https://doi.org/10.1111/j.1365-246X.1982.tb04976.x>.
- [56] A. Hoehner, S.V. Sobolev, I. Einarsson, R. Wang, Investigation on afterslip and steady state and transient rheology based on postseismic deformation and geoid change caused by the sumatra 2004 earthquake, G-cubed 12 (2011), <https://doi.org/10.1029/2010gc003450> n/a–n/a.
- [57] I. Jackson, J.D. Fitz Gerald, U.H. Faul, B.H. Tan, Grain-size-sensitive seismic wave attenuation in polycrystalline olivine, *J. Geophys. Res. Solid Earth* 107 (2002), <https://doi.org/10.1029/2001JB001225>. ECV–5.
- [58] C. Goetze, High temperature rheology of westerly granite, *J. Geophys. Res.* 76 (1971) 1223–1230, <https://doi.org/10.1029/JB076i005p01223>.
- [59] C. Goetze, W. Brace, Laboratory observations of high-temperature rheology of rocks, *Dev. Geotectonics* 4 (1972) 583–600, <https://doi.org/10.1016/B978-0-444-41015-3.50036-7>. Elsevier.
- [60] F.F. Pollitz, R. Bürgmann, P. Banerjee, Postseismic relaxation following the great 2004 sumatra-andaman earthquake on a compressible self-gravitating earth, *Geophys. J. Int.* 167 (2006) 397–420, <https://doi.org/10.1111/j.1365-246X.2006.03018.x>.

- [61] J.A. Clark, W.E. Farrell, W.R. Peltier, Global changes in postglacial sea level: a numerical calculation, *Quat. Res.* 9 (1978) 265–287.
- [62] J.A. Clark, The reconstruction of the laurentide ice sheet of north America from sea level data: method and preliminary results, *J. Geophys. Res. Solid Earth* 85 (1980) 4307–4323, <https://doi.org/10.1029/JB085iB08p04307>.
- [63] G. Spada, D. Melini, Selen 4 (selen version 4.0): a fortran program for solving the gravitationally and topographically self-consistent sea-level equation in glacial isostatic adjustment modeling, *Geosci. Model Dev. (GMD)* 12 (2019) 5055–5075, <https://doi.org/10.5194/gmd-12-5055-2019>.
- [64] A.J. Weaver, O.A. Saenko, P.U. Clark, J.X. Mitrovica, Meltwater pulse 1a from Antarctica as a trigger of the bølling-allerød warm interval, *Science* 299 (2003) 1709–1713, <https://doi.org/10.1126/science.1081002>.
- [65] Y. Lin, F.D. Hibbert, P.L. Whitehouse, S.A. Woodroffe, A. Purcell, I. Shennan, S.L. Bradley, A reconciled solution of meltwater pulse 1a sources using sea-level fingerprinting, *Nat. Commun.* 12 (2021) 2015, <https://doi.org/10.1038/s41467-021-21990-y>.
- [66] F. Rémy, T. Flament, A. Michel, J. Verron, Ice sheet survey over Antarctica using satellite altimetry: Ers-2, envisat, saral/altika, the key importance of continuous observations along the same repeat orbit, *Int. J. Rem. Sens.* 35 (2014) 5497–5512, <https://doi.org/10.1080/01431161.2014.926419>.
- [67] L. Schröder, M. Horwath, R. Dietrich, V. Helm, M.R. Van Den Broeke, S.R. Ligtenberg, Four decades of antarctic surface elevation changes from multi-mission satellite altimetry, *Cryosphere* 13 (2019) 427–449, <https://doi.org/10.5194/tc-13-427-2019>.
- [68] R.E. Riva, B.C. Gunter, T.J. Urban, B.L. Vermeersen, R.C. Lindenbergh, M.M. Helsen, J.L. Bamber, R.S. van de Wal, M.R. van den Broeke, B.E. Schutz, Glacial isostatic adjustment over Antarctica from combined icesat and grace satellite data, *Earth Planet Sci. Lett.* 288 (2009) 516–523, <https://doi.org/10.1016/j.epsl.2009.10.013>.
- [69] P.L. Whitehouse, M.J. Bentley, G.A. Milne, M.A. King, I.D. Thomas, A new glacial isostatic adjustment model for Antarctica: calibrated and tested using observations of relative sea-level change and present-day uplift rates, *Geophys. J. Int.* 190 (2012) 1464–1482, <https://doi.org/10.1111/j.1365-246X.2012.05557.x>.
- [70] E.R. Ivins, T.S. James, J. Wahr, O. Schrama, J. E. F.W. Landerer, K.M. Simon, Antarctic contribution to sea level rise observed by grace with improved gia correction, *J. Geophys. Res. Solid Earth* 118 (2013) 3126–3141, <https://doi.org/10.1002/jgrb.50208>.
- [71] G. A. J. Wahr, S. Zhong, Computations of the viscoelastic response of a 3-D compressible Earth to surface loading: an application to Glacial Isostatic Adjustment in Antarctica and Canada, *Geophys. J. Int.* 192 (2013) 557–572, <https://doi.org/10.1093/gji/ggs030>.
- [72] C. Zhao, M.A. King, C.S. Watson, V.R. Barletta, A. Bordoni, M. Dell, P.L. Whitehouse, Rapid ice unloading in the fleming glacier region, southern antarctic peninsula, and its effect on bedrock uplift rates, *Earth Planet Sci. Lett.* 473 (2017) 164–176, <https://doi.org/10.1016/j.epsl.2017.06.002>.
- [73] S. Adhikari, G.A. Milne, L. Caron, S.A. Khan, K.K. Kjeldsen, J. Nilsson, E. Larour, E.R. Ivins, Decadal to centennial timescale mantle viscosity inferred from modern crustal uplift rates in Greenland, *Geophys. Res. Lett.* 48 (2021), <https://doi.org/10.1029/2021gl094040>.

**Alexandre Boughanemi** is PhD student at Université Côte d'Azur since 2021. He received his master's degree in geophysics in 2021 at Université Côte d'Azur. He studies the glacial isostatic adjustment in Antarctica, using a multi-technic approach to inverse a surface displacement model.

**Anthony Mémin** received his PhD in gravimetry and geodesy from Université de Strasbourg, France, in 2011. He is an Associate Professor at Université Côte d'Azur, Nice, France, since 2014. He studies the response of the solid Earth in terms of surface deformation and gravity variations induced by daily to millennia surface mass redistributions.